Forsch Ingenieurwes (2023) 87:219–226
https://doi.org/10.1007/s10010-023-00638-x

ORIGINALARBEITEN/ORIGINALS

# Impact of DC link brake chopper design on the LVRT behavior of full-scale converter wind turbines

**Fabian Herzog**[1] · **Julian Röder**[2] · **Rik W. De Doncker**[1]

Received: 31 October 2022 / Accepted: 21 January 2023 / Published online: 20 March 2023


**Abstract**
Wind turbines (WTs) are loaded by the wind and by the electrical grid. A low voltage ride through (LVRT) is a special load case for WTs, which can be critical for their drivetrain. They are usually less severe for WTs with a full-scale converter (FSC); however, in some cases there are still loads observable in the mechanical drivetrains of WTs with FSCs. Different aspects like the brake chopper design, the control and specifications of the grid side converter (GSC) as well as the grid and fault parameters affect these loads. In this paper, three different LVRT behaviors of a WT with a squirrel-cage induction generator (SCIG) and a FSC were investigated via simulations. In the worst case, a sharp peak in the electromagnetic torque of the generator after fault clearance is possible. The cause lies in the GSC control, especially the phase-locked loop (PLL), and can also be influenced by adjusting the control parameters, brake chopper and filter design. The resulting mechanical drivetrain torque, on the other hand, is increased by only 2.9% for a very short time. Thus, the loading of the mechanical drivetrain components is only slightly increased. Therefore, the risk of damage to the mechanical components of the FSC WT due to grid faults is relatively low.

## Auswirkung der Auslegung des Zwischenkreisbremschoppers auf das LVRT-Verhalten von Windenergieanlagen mit Vollumrichter

**Zusammenfassung**
Windenergieanlagen (WEA) werden durch den Wind und durch das Stromnetz belastet. Ein Low-Voltage-Ride-Through (LVRT) ist ein spezieller Lastfall für WEA, der für ihren Antriebsstrang kritisch sein kann. Bei WEA mit Vollumrichter (FSC) sind sie in der Regel weniger gravierend; in einigen Fällen sind dennoch Belastungen im mechanischen Antriebsstrang von WEA mit FSC zu beobachten. Verschiedene Aspekte wie das Design des Bremschoppers, die Regelung und die Spezifikationen des netzseitigen Umrichters (GSC) sowie die Netz- und Fehlerparameter beeinflussen diese Belastungen. In diesem Beitrag wurden drei verschiedene LVRT-Verhaltensweisen einer WEA mit einem Asynchrongenerator mit Kurzschlussläufer (SCIG) und einem FSC mittels Simulationen untersucht. Im ungünstigsten Fall ist eine starke Spitze im elektromagnetischen Drehmoment des Generators nach der Fehlerbeseitigung möglich. Die Ursache liegt in der GSC-Regelung, insbesondere der Phasenregelschleife (PLL), und kann auch durch Anpassung der Regelparameter, des Bremschoppers und der Filterauslegung beeinflusst werden. Das resultierende mechanische Antriebsstrangmoment wird dagegen sehr kurzzeitig um nur 2,9 % erhöht. Die Belastung der mechanischen Komponenten des Antriebsstrangs wird also nur geringfügig erhöht. Daher ist das Risiko einer Beschädigung der mechanischen Komponenten des FSC WT aufgrund von Netzfehlern relativ gering.

✉ Fabian Herzog
post_pgs@eonerc.rwth-aachen.de

[1] Institute for Power Generation and Storage Systems, Mathieustr. 10, 52074 Aachen, Germany

[2] Chair for Wind Power Drives, Campus Boulevard 61, 52074 Aachen, Germany

## 1 Introduction

Wind energy plays a key role in the energy system today. A high share of WTs in Germany is built with FSCs [1] because of their high reliability and flexibility [2]. The most common concepts of WTs with FSCs are with an electrically excited synchronous generator, a permanent magnet

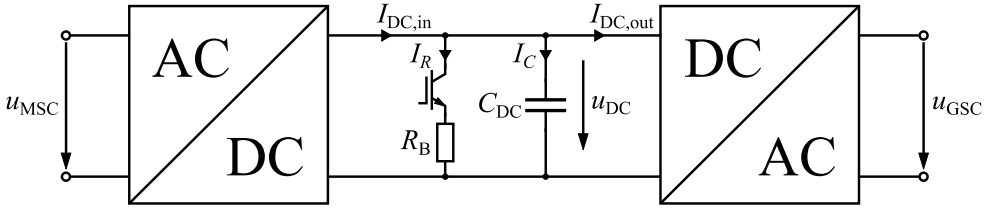


**Fig. 1** Simplified circuit for analysis

synchronous generator and with a SCIG. In this paper, the focus is on the investigation of grid faults with an SCIG and the influence of the brake chopper.

LVRT tests are conducted to investigate the behavior of WTs during grid faults like a short circuit. An LVRT introduces high loading to the power-electronic converter system. In order to protect the converter from over-voltages, brake chopper resistors are used to convert excess power into heat and reduce the voltage dynamics of the DC link [3]. A power electronic switch, usually an insulated gate bipolar transistor (IGBT), turns the brake chopper on and off.

Power converter faults have been investigated for WTs with SCIG and with doubly-fed induction generators (DFIG) [4–6]. They lead to high electrical and mechanical loads, which can damage the mechanical drivetrain and electrical components. However, grid faults have been thoroughly investigated with WTs with DFIGs, which use a partial-scale converter [3, 7]. In contrast to DFIGs, a grid voltage drop with SCIGs has nearly no influence on the mechanical drivetrain of the WT. However, mechanical loads can be introduced in specific cases, which depend on parameters of the filter, brake chopper and control design. In this paper will be investigated if adjustments of the brake chopper and control design have influences on the electromagnetic torque of the generator and therefore the loading of the mechanical drivetrain during LVRTs of a WT with a FSC.

## 2 Theory

The behavior of the DC link voltage during short circuit faults in the medium voltage (MV) grid is introduced. In the following, losses in the generator and the power semiconductors are neglected. Therefore, the simplified circuit as shown in Fig. 1 is analyzed. All relevant currents, voltages and passive elements are labeled.

The maximum current supplied to the short circuit depends on the limit $i_{AC,max}$ set in the converter control. This results in a maximum power $P_{SC,GSC}$ which the grid side converter (GSC) can supply to the grid which can be calculated using Eq. 1.

$$P_{SC,\mathrm{GSC}} = 3 \cdot R_G \cdot {i_{AC,\mathrm{max}}}^2 \tag{1}$$

Here, $R_G$ is the resistance seen from the converter into the grid. This leads to a maximum DC current $i_{DC,out}$ which the GSC can draw from the DC link which is dependent on the DC link voltage $u_{DC}$ and $P_{SC,GSC}$ according to active-power balance. Therefore, $i_{DC,out}$ can be calculated using Eq. 2.

$$i_{\mathrm{DC,out}} = \frac{3 \cdot R_G \cdot {i_{\mathrm{AC,max}}}^2}{u_{\mathrm{DC}}} \tag{2}$$

The input current into the DC link drawn from the generator by the machine side converter (MSC) can be calculated from the operating point of the generator according to Eq. 3.

$$i_{\mathrm{DC},in} = \frac{2\pi n T}{u_{\mathrm{DC}}} \tag{3}$$

Here, $n$ is the mechanical rotational speed and $T$ the electromagnetic torque of the generator. The difference between the maximum current fed into the grid $i_{DC,out}$ and the input current $i_{DC,in}$ yields the current of the DC link capacitor $i_C$. This current charges and discharges the DC link capacitor $C_{DC}$ and therefore determines the DC link voltage according to Eq. 4.

$$i_C = i_{DC,in} - i_{DC,\mathrm{out}} = C_{DC} \frac{d u_{DC}}{dt} \tag{4}$$

**Table 1** Specifications of the full-scale converter

| Parameter | Value |
|---|---|
| Switching frequency | $f_{SW} = 2.5\,\mathrm{kHz}$ |
| Max. GSC current | $\hat{i}_{AC,max} = 4000\,\mathrm{A}$ |
| DC link capacitance | $C_{DC} = 35.3\,\mathrm{mF}$ |
| Nominal DC link voltage | $U_{DC,N} = 1100\,\mathrm{V}$ |
| Filter inductor | $L_{LC} = 200\,\mu\mathrm{H}$ |
| Filter capacitor | $C_{LC} = 800\,\mu\mathrm{F}$ |
| Brake chopper resistance | $R_B = 290\,\mathrm{m\Omega}$ |

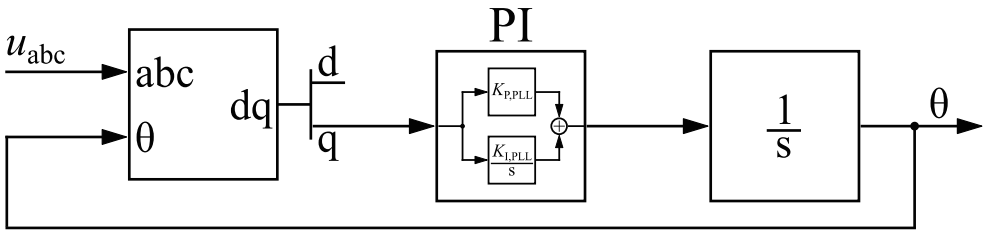


**Fig. 2** Block diagram of a synchronous reference frame PLL

Here, $C_{DC}$ is the DC link capacitance of the converter. When the brake chopper starts conducting, $i_C$ is reduced significantly by the current $i_R$ through the brake chopper resistance $R_B$ as can be seen in Eq. 5.

$$i_R = i_{DC,in} - i_C - i_{DC,out} = \frac{u_{DC}}{R_B} \tag{5}$$

When the current $i_R$ exceeds the difference of $i_{DC,in}$ and $i_{DC,out}$, the voltage across $C_{DC}$ drops. Otherwise, the brake chopper resistance $R_B$ was chosen too large so that the excess power from the generator cannot be converted into heat and therefore will charge the capacitor. In this case, the capacitor voltage will increase which leads to an increase of the current $i_R$. In turn, $i_C$ decreases until $i_R$ exceeds the difference of $i_{DC,in}$ and $i_{DC,out}$ so that a constant voltage $U_{DC,max}$ will be reached. This maximum voltage can be calculated using Eq. 6. Finally, when the fault is cleared, the grid voltage will recover. Ideally, the DC link voltage will decrease to its nominal value and the GSC control starts working under normal conditions, again.

$$\begin{aligned} U_{DC,\max} &= R_B \cdot \left(i_{DC,in} - i_{DC,\max}\right) \\ &= \sqrt{R_B \cdot \left(2\pi n T - 3 \cdot R_G \cdot {i_{AC,\max}}^2\right)} \end{aligned} \tag{6}$$

**Table 2** Specifications of the generator

| Parameter | Value |
|---|---|
| Nominal power | $P_N = 2.75\,\text{MW}$ |
| Nominal torque | $T_N = 24.7\,\text{kNm}$ |
| Pole pairs | $p_P = 3$ |
| Rotor and stator winding resistance | $R_S = R_R' = 1.5\,\text{m}\Omega$ |
| Stator inductance | $L_S = 84.7\,\mu\text{H}$ |
| Rotor inductance | $L_R' = 81.8\,\mu\text{H}$ |

A nacelle transformer in Dy7 configuration connects the WT with a three-phase 20 kV medium voltage (MV) grid. A series RL impedance is used to represent the low voltage (LV) and MV grid. The three phase short circuit modelling a grid fault is implemented on the MV grid close to the nacelle transformer using ideal switches and a fault resistance of $R_f = 1\,\text{m}\Omega$ as shown in Fig. 3.

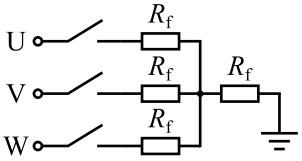


**Fig. 3** Modelling of the three-phase short circuit fault

## 3 Methodology

The simulation model is implemented in MATLAB Simulink. The full-scale converter of the SCIG is implemented using ideal switching devices. The GSC includes an LC filter whereas no filters are used on the machine side. The converter specifications are chosen similar to the specifications of an existing full-scale wind turbine converter and are shown in Table 1.

The GSC is controlled with a cascaded control algorithm for WT converters that controls the DC link voltage and the reactive power fed into the grid [8]. The grid phase angle is detected by a synchronous reference frame phase locked loop (PLL) [9], as shown in Fig. 2. The voltage controller includes an anti-windup using the back-calculation method with the coefficient $K_{b,GSC}$ [10]. An indirect rotor-flux oriented control scheme is used on the MSC to control torque and rotor flux of the SCIG [8]. The brake chopper IGBT of the converter is controlled with a hysteresis controller which turns on at a voltage level of $U_{DC,on} = 1.13 \cdot U_{DC,N} = 1243\,\text{V}$ and turns off at a voltage of $U_{DC,off} = 1.07 \cdot U_{DC,N} = 1177\,\text{V}$.

A generator model of an existing generator available at the Center for Wind Power Drives (CWD) of RWTH Aachen was used. The generator model is implemented using an electrical state-space model for asynchronous machines. The generator parameters are taken from the datasheet and equivalent circuit diagram provided by the manufacturer. The specifications of the generator are shown in Table 2.

## 4 Results

In the following, different simulations were conducted to see the behavior of the DC link and its influence on the

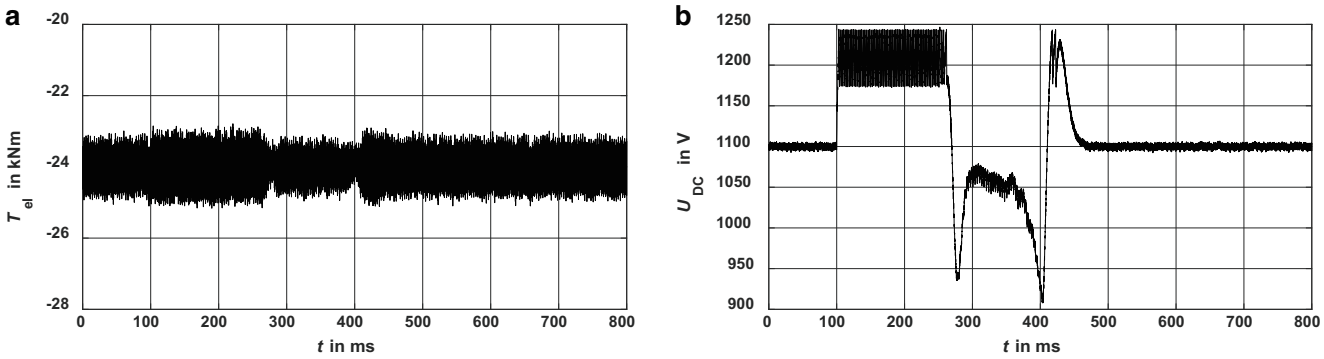


**Fig. 4** Electromagnetic torque of the generator and DC link voltage of the converter. **a** Electromagnetic torque. **b** DC link voltage

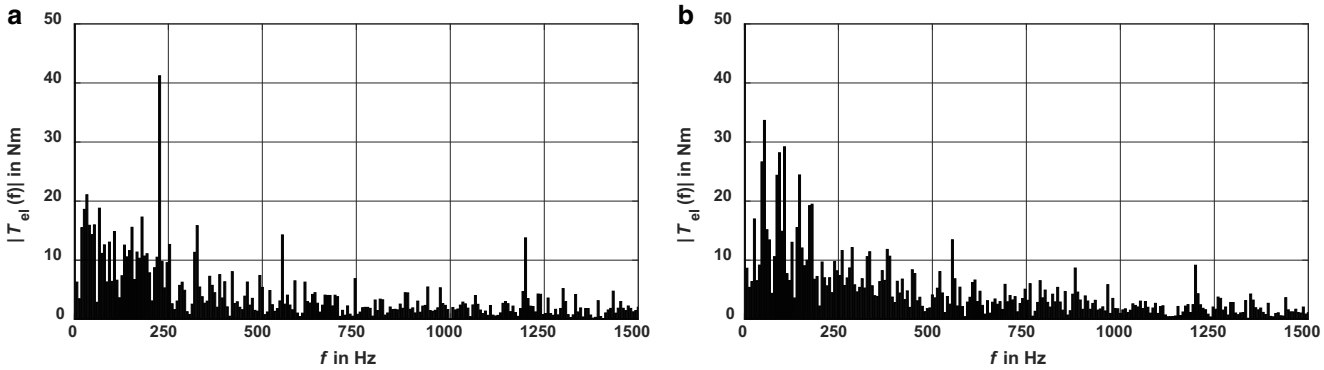


**Fig. 5** Frequency spectrum of the electromagnetic torque. **a** Spectrum during normal operation. **b** Spectrum during fault

electromagnetic torque of the generator in specific situations. Three cases were investigated. In the first case the previously described parameter settings were used which results in a normal brake chopper operation. In the second case the brake chopper resistance $R_B$ is increased which results in a lower power dissipation of the chopper. For the third case the anti-windup of the GSC controller was adjusted which results in a dynamic generator torque excitation. Additionally, different parameters influencing the torque behavior for insufficient anti-windup were identified and varied.

The WT is working at its nominal operating point with a speed of 1100 rpm and a torque of 24 kNm. After 100 ms, an LVRT event is simulated using a short circuit fault, which is cleared after a fault duration of 150 ms. This operating point and fault condition was chosen because here the WT is generating the largest power output while minimal power can be fed into the grid. Therefore, this is the most critical situation for a brake chopper since it is the largest possible excess power.

### 4.1 Case I

In the first case, the parameter settings of the WT as described in the previous chapter were used. Figure 4 shows the electromagnetic torque and the DC link voltage during and after the fault. When the chopper turns on shortly after the fault, the DC link voltage immediately drops until it reaches $U_{DC,off}$. Hence, the brake chopper is able to dissipate the excess power of the WT. Thereafter, the DC link voltage increases again until the chopper turns on at $U_{DC,on}$. The DC link voltage waveform for this case is shown in Fig. 4b. As can be seen, a triangular voltage results with a maximum of $U_{DC,on}$ and a minimum of $U_{DC,off}$. The frequency of the voltage $f_T$ can be approximated by Eq. 8, which can be derived from Eqs. 5 and 6.

$$\frac{1}{f_T} = t = \left(U_{DC,on} - U_{DC,\mathrm{off}}\right) \cdot C_{DC} \cdot \left(\frac{1}{i_{DC,in} - i_{DC,\mathrm{out}}} - \frac{1}{i_{DC,in} - i_R - i_{DC,\mathrm{out}}}\right) \tag{7}$$

The frequency reaches 416 Hz for the given parameters and operating point. During the fault, the PLL of the GSC loses the synchronization to the voltage phase angle of the electrical grid. Thus, a small tracking error appears during the fault, which is still present for a short time after the fault. Therefore, the GSC is not able to supply the correct current to the grid, which results in an error in the DC link voltage control until the phase tracking of the PLL is synchronized

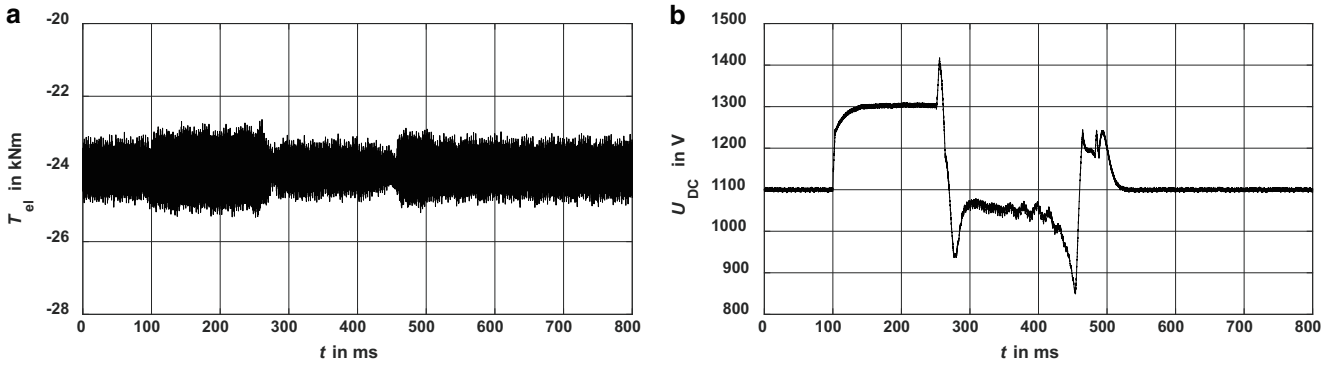


**Fig. 6** Electromagnetic torque of the generator and DC link voltage of the converter. **a** Electromagnetic torque. **b** DC link voltage

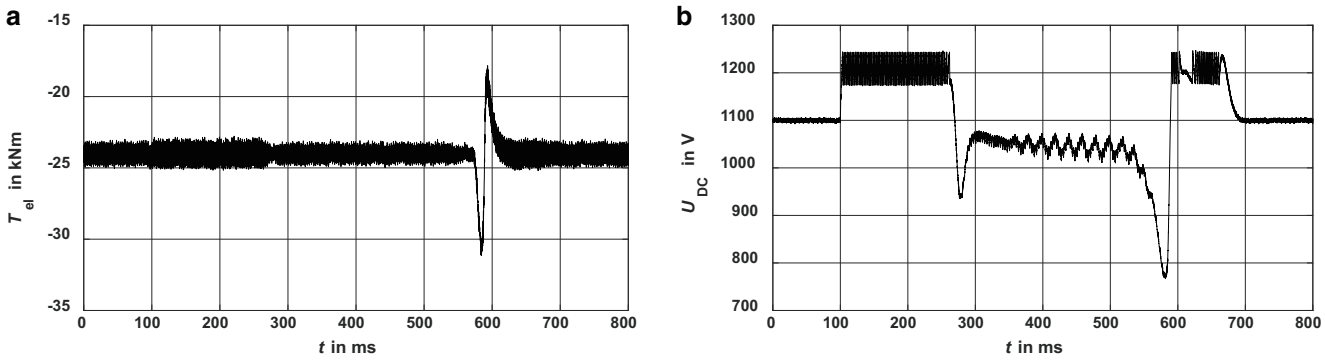


**Fig. 7** Electromagnetic torque of the generator and DC link voltage of the converter. **a** Electromagnetic torque. **b** DC link voltage

again. This behavior can be seen in Fig. 4b between 250 and 400 ms. Alternatively, the GSC could reduce its output current until it is synchronized again. That would result in the chopper being active for a longer duration, but $U_{DC}$ would stay above its nominal value and the grid distortion of the GSC would be reduced.

Figure 4a shows the electromagnetic torque of the generator. Again, a small increase of the torque ripple is visible during the fault. Otherwise, there is no major peak or ripple identifiable. A closer look at the frequency spectrum of the electromagnetic torque during normal operation and during a fault is shown in Fig. 5. Here, an increase in the frequency range of $f_T = 416$ Hz could be possible. However, due to the much higher switching frequency of the converter compared to $f_T$ and the sufficiently high control bandwidth no such influence can be observed.

## 4.2 Case II

For the second case a large brake chopper resistance is chosen $R_B$ which reduces the chopper current $i_R$ and therefore the maximum power dissipation of the brake chopper. When $R_B$ is chosen too large, the brake chopper may not be able to dissipate the excess power from the WT during a grid fault. Rearranging Eq. 6, a formula for the maximum possible brake chopper resistance $R_{B,max}$ can be derived which is shown in Eq. 7.

$$R_{B,\max} = \frac{{U_{DC,\text{off}}}^2}{2\pi nT - 3R_G {i_{AC,\max}}^2} \tag{8}$$

Here, $U_{DC,off}$ is the lower voltage of the hysteresis band of the hysteresis controller of the brake chopper IGBT. With the parameters used in this paper the maximum possible brake chopper resistance $R_{B,max}$ for a sufficient power dissipation is approximately 655 mΩ.

When a larger resistance is chosen, the capacitor gets charged to a voltage larger than $U_{DC,off}$ and can damage the converter. Figure 6b shows the DC link voltage during the short circuit fault for a chopper resistance of $R_B = 800$ mΩ. It can be seen that the capacitor gets charged rapidly until the brake chopper turns on which then slows down the charging speed until a steady state voltage is reached. This voltage can be calculated using Eq. 6. It is higher than the turn on voltage of the chopper $U_{DC,on}$ which usually is close to the maximum voltage for most of the components of the converter. Thus, this case may lead to damages in the converter, especially in the DC link capacitors and the IGBTs. Figure 6a shows the electromagnetic torque of the

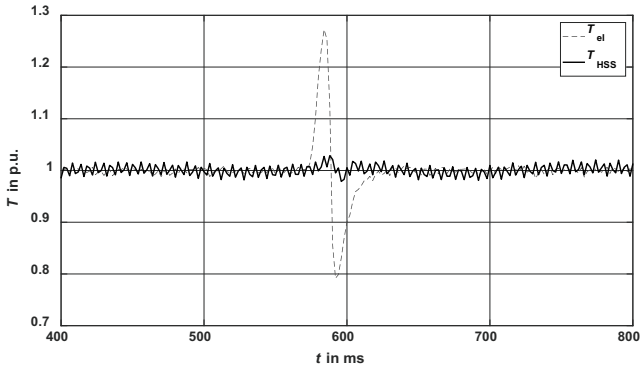


**Fig. 8** Electromagnetic torque of the generator and the HSS after the fault

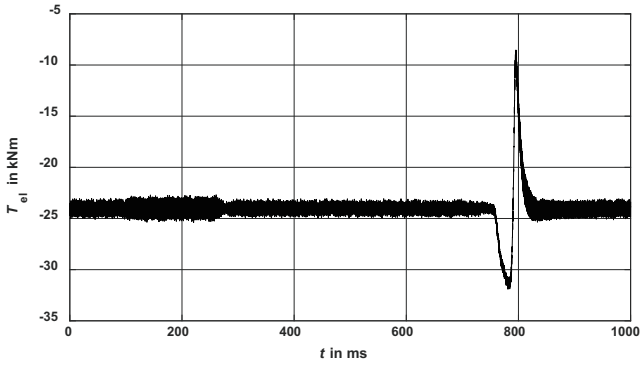


**Fig. 9** Electromagnetic torque with an increased brake chopper resistance

generator where only a small increase of the torque ripple is visible during the fault.

Although this case does not directly lead to dynamic torque excitations, the overvoltage can result in short circuit faults in the converter. Subsequently, this leads to highly dynamic torque excitations surpassing four times the nominal torque of the wind turbine and increasing the risk for damage of the mechanical drivetrain [4, 5]. In practice, this case can be avoided by using much smaller brake chopper resistances than necessary.

### 4.3 Case III

The third case is the only investigated case that directly leads to a significant generator torque excitation. For this case, the anti-windup back-calculation coefficient $K_{b,GSC}$ of the voltage controller of the GSC was reduced from 10 to 1.

As can be seen from Fig. 7a, a peak in the electromechanical torque results after the LVRT. As shown earlier, the PLL loses the synchronization to the voltage phase angle of the electrical grid. Therefore, voltages and currents from the GSC are distorted and the control is not working as intended. Hence, the DC link voltage controller is not able to set the correct voltage, as can be seen in Fig. 7b. When the PLL synchronizes again, the current of the GSC is comparably high which leads to a voltage drop of $U_{DC}$. This voltage drop may lead to an increase of the MSC currents when they drop below a certain value, which is dependent on the operating point of the generator. This results in a sharp increase of the generator torque followed by a sudden decrease.

The resulting loads on the mechanical drivetrain are investigated using a multi-body simulation (MBS) model as described in [4]. Figure 8 shows the electromagnetic torque of the generator and the resulting torque at the high-speed shaft (HSS) of the WT in p.u. After the peak in the generator torque $T_{el}$ only a small increase and decrease in the torque of the HSS $T_{HSS}$ can be seen. The peak is dampened from 27% at the generator to 2.9% at the HSS due to the large inertia of the drivetrain. Therefore, no damages in the mechanical drivetrain are expected due to the small influence on $T_{HSS}$.

Several parameters have an influence on the appearance and the value of the torque peak. Therefore, more investigations are necessary to verify that even with the variation of different parameters no critical peaks can be found.

First, the influence of the brake chopper parameters is investigated. Varying the resistance value of the brake chopper has shown no significant impact until the maximum

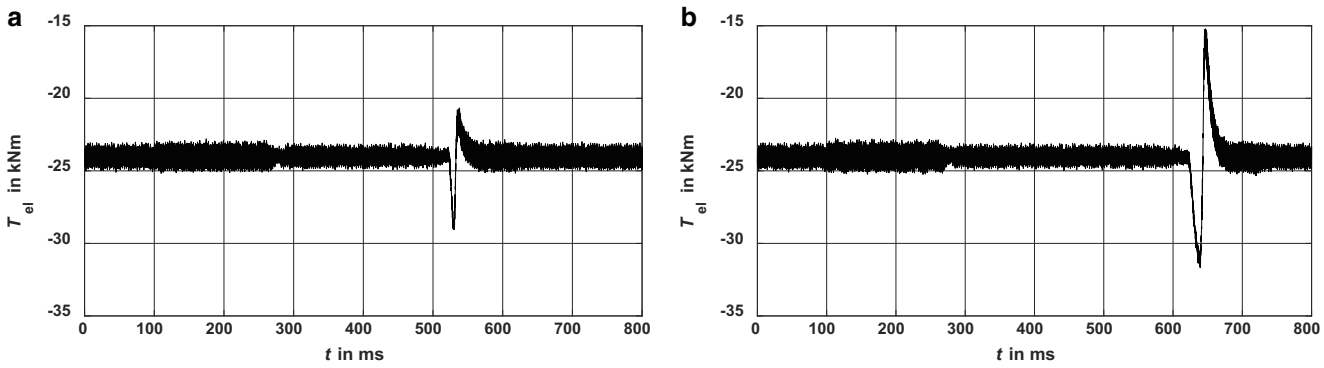


**Fig. 10** Electromagnetic torque with changed hysteresis parameters of the brake chopper. **a** Reduction of hysteresis parameters. **b** Increase of hysteresis parameters

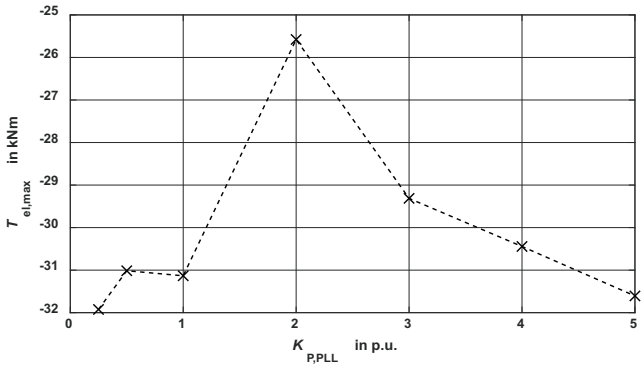


**Fig. 11** Maximum electromagnetic torque peak depending on the proportional gain of the PLL

brake chopper resistance $R_{B,max}$ is reached. Thereafter, the reverse peak increases significantly with increasing $R_B$, as can be seen in Fig. 9. Here, a brake chopper resistance of $R_B = 800\ m\Omega$ was chosen.

Thereafter, the parameters of the hysteresis controller of the brake chopper were varied. Figure 10a shows the electromagnetic torque of the generator for a reduction of $U_{DC,on}$ from $1.13 \cdot U_{DC,N}$ to $1.11 \cdot U_{DC,N}$ and $U_{DC,off}$ from $1.07 \cdot U_{DC,N}$ to $1.05 \cdot U_{DC,N}$. Here, a significant reduction of the torque peak is visible. However, increasing the turn on and turn off values of the chopper from $1.13 \cdot U_{DC,N}$ to $1.15 \cdot U_{DC,N}$ and $U_{DC,off}$ from $1.07 \cdot U_{DC,N}$ to $1.09 \cdot U_{DC,N}$ an increase of the peak, especially the reverse peak, can be seen, as shown in Fig. 10b. This implies that lower values for the hysteresis controller are beneficial. However, low values can lead to false turn-on commands of the brake chopper during dynamic load changes.

Afterwards, the influence of the bandwidth of the PLL is investigated. Figure 11 shows the maximum torque peak $T_{el,max}$ for different values of the proportional gain $K_{P,PLL}$ of the PLL. Doubling the gain compared to the normal value of $K_{P,PLL} = 1$ p.u. results in the lowest peak, while increasing or decreasing the value further increases $T_{el,max}$. However, since the gain of the PLL influences the speed and precision of the detection of the grid phase angle as well as its rejection of grid disturbances, a careful evaluation of the parameter is necessary [11].

Additionally, parameters, which benefit the overflow of the PI controller of the DC link voltage control of the GSC increase the torque peak. Especially, reducing or removing the anti-windup or increasing the I gain of the GSC voltage controller increase the peak slightly. In addition, the AC-filter design has an effect on the peak. Increasing the filter inductance $L_f$ increases the torque peak, while increasing the filter capacitance $C_f$ decreases the torque peak slightly. Lastly, an increase of the DC link capacitance $C_{DC}$ increases the peak slightly.

The dynamic of the electromagnetic torque in the different investigations in the third case is comparable and the peak is only slightly changed compared to the behavior shown in Fig. 8. Therefore, the risk of damage in the mechanical drivetrain of the wind turbine stays low.

## 5 Summary and conclusion

A simulative investigation of the impact of the brake chopper design on the LVRT behavior of FSC WTs with a SCIG was presented. Three different scenarios were shown and the behavior of the electromagnetic torque of the generator and of the DC link voltage was analyzed. In the first case a normal chopper operation was analyzed. There were no impacts on the electromagnetic torque of the generator visible except for a slightly increased ripple caused by the increased DC link voltage. An analysis of the spectrum of the electromagnetic torque has shown no increase in specific frequencies which could be expected because of the triangular DC link voltage.

For the second case the brake chopper resistance was increased and the brake chopper was not able to dissipate the excess power anymore. There was no direct impact on the electrical and mechanical drivetrain visible besides the increased risk of damage to the electrical drivetrain caused by the overvoltage. However, the consequence of an overvoltage in the power converter can lead to short circuit faults which result in highly dynamic torque excitations and thus in an increased risk of damage of the mechanical drivetrain.

For the third case the anti-windup of the GSC controller was adjusted which resulted in a dynamic peak of the electromagnetic torque of the generator. A detailed analysis of the loading on the mechanical drivetrain during the fault has shown that the loading at the HSS is only increased by 2.9%. Thereafter, different parameters, which influence the resulting peak, were investigated. It was shown that the parameters of the hysteresis controller and the bandwidth of the PLL have an influence on the peak and may increase it. However, the dynamic of the electromagnetic torque is only changed slightly while varying the parameters within reasonable ranges. Hence, damages of the mechanical drivetrain in this case are unlikely.

Compared to grid faults with DFIGs, where loads of double the nominal torque appear, the mechanical loading is much less severe with SCIGs. Additionally, the peaks only appear for a short timeframe and therefore are mostly dampened by the high inertia of the mechanical drivetrain of the WT.

**Acknowledgements** The authors would like to thank the Ministry of Economic Affairs, Innovation, Digitalization and Energy of the State of North Rhine-Westphalia, Germany, for the financial support granted.

They also thank their project partners for the equipment, insight as well as expertise they have provided, which contributed to this joint project.


**Funding** Open Access funding enabled and organized by Projekt DEAL.



## References

1. Fraunhofer IEE (2018) Windenergie Report Deutschland. https://publica.fraunhofer.de/bitstreams/67c3f1d8-8085-4ed4-8b4b-49dd7b52ef58/download. Accessed 10 Nov 2022
2. Yaramasu V, Wu B, Sen PC, Kouro S, Narimani M (2015) High-power wind energy conversion systems: State-of-the-art and emerging technologies. Proc IEEE 103(5):740–788
3. Erlich I, Wrede H, Feltes C (2007) Dynamic behavior of DFIG-based wind turbines during grid faults. 2007 Power Conversion Conference, Nagoya, pp 1195–1200
4. Röder J, Jacobs G, Duda T, Bosse D, Herzog F (2021) Simulative investigation of wind turbine gearbox loads during power converter fault. Forsch Ingenieurwes 85(2):251–256
5. Röder J, Jacobs G, Duda T, Bosse D, Herzog F (2021) Investigation of dynamic loads in wind turbine drive trains Due to grid and power converter faults. Energies 14(24):8542
6. Röder J, Jacobs G, Bosse D, Herzog F, Graf L (2022) Investigation of a converter fault for a DFIG wind turbine and analysis of the resulting gearbox component loads. J Phys Conf Ser 2257(1):12013
7. Herzog F, Röder J, Frehn A, Ruhe N, De Doncker RW (2022) Influences on the LVRT behavior of DFIG wind turbine systems. J Phys Conf Ser 2265(2):22075
8. Wu B, Lang Y, Zargari N, Kouro S (2011) Power conversion and control of wind energy systems. IEEE Press series on power engineering 74. Wiley & Sons, Hoboken
9. Kaura V, Blasko V (1997) Operation of a phase locked loop system under distorted utility conditions. IEEE Trans on Ind Applicat 33(1):58–63
10. Bohn C, Atherton DP (1995) An analysis package comparing PID anti-windup strategies. IEEE Control Syst Mag 15(2):34–40
11. Liserre M, Rodriguez P, Teodorescu R (2011) Grid converters for photovoltaic and wind power systems. Wiley, Hoboken